Applied Catalysis B: Environmental 257 (2019) 117905

Contents lists available at ScienceDirect

Applied Catalysis B: Environmental

journal homepage: www.elsevier.com/locate/apcatb

Carbon dots-Pt modified polyaniline nanosheet grown on carbon cloth as stable and high-efficient electrocatalyst for hydrogen evolution in pH-universal electrolyte

Qian Dang, Yuyang Sun, Xiao Wang, Wenxiang Zhu, Ying Chen, Fan Liao, Hui Huang*, Mingwang Shao*

Institute of Functional Nano & Soft Materials (FUNSOM), Jiangsu Key Laboratory for Carbon-Based Functional Materials & Devices, Soochow University, Suzhou 215123, PR China

ARTICLE INFO

Keywords:
Carbon dots (CDs)
Polyaniline (PANI)
Hydrogen evolution reaction (HER)
Electrocatalysis
pH-universal

ABSTRACT

Design and fabrication of hydrogen evolution reaction (HER) electrocatalysts with high activity, durability and moderate price are vital for realizing a viable water-splitting technology. Here, we demonstrate the carbon dots-Pt modified polyaniline nanosheets grown on carbon cloth (CDs/Pt-PANI) can serve as stable and high-efficient electrocatalyst in pH-universal electrolyte for HER. The overpotential for optimal CDs/Pt-PANI electrocatalyst can be lowered to 30 mV at 10 mA·cm^{-2} when Pt loading was only 8.1 μg·cm^{-2} (the Pt content in commercial 20 wt% Pt/C is 22.4 μg·cm^{-2}), showing exceptional HER efficiency with a small Tafel slope 41.7 mV·dec^{-1} in acidic solution. Meanwhile, the optimal CDs/Pt-PANI electrocatalyst exhibits well stability with 17 mV potential shift after 20 h, which is 0.06 times than that of commercial 20 wt% Pt/C (286 mV). It is noticeable, the optimal CDs/Pt-PANI electrocatalyst is superior to 20 wt% Pt/C with HER performance in pH-universal electrolyte (acidic, neutral and basic). The efficient and stable HER performance of CDs/Pt-PANI should ascribe to the synergy in the CDs, Pt and PANI, in which the surface functional groups of CDs can connect tightly with PANI and improve the stability of Pt, simultaneously, the PANI and Pt provide the high-efficiency in HER.

1. Introduction

Environment pollution and energy crisis drive people's interest on the clean and renewable energy sources. Hydrogen is considered to be the most promising energy source with zero-pollution emission [1–5]. A clean and efficient method for H_2 production is electrolysis of water with the aid of electrocatalysts, which are supposed to lower the energy consumption and accelerate the reaction rate. Platinum (Pt) group metals are viewed as the most efficient catalysts for hydrogen evolution reaction (HER) [6–10]. However, the scarcity of Pt makes it impractical for global scale applications. Additionally, the poor stability of noble metal based catalysts is severe [11–15]. Therefore, it is highly desirable to develop low-cost and high-efficiency electrocatalysts in pH-universal electrolytes for HER.

There are two strategies to improve the electrocatalytic activity and stability of the electrocatalysts: One is to employ the non-noble metal materials, such as metal oxides [16], sulfides [17], phosphides [18], and their large surface area may provide high density of active sites. However, their electrocatalytic activities are usually lower than Pt-based catalysts. The other is to reduce the content of Pt and choose suitable substrates, which will preserve the electrocatalytic activity and further improved the stability [19]. And a promising catalyst system should expose more active sites, promote mass diffusion and accelerate of electron transfer [20,21].

Carbon dots (CDs) with the size less than 10 nm show excellent properties in optics and electronics. CDs with the oxygen-rich functional groups can regarded as the active component to construct composites for strengthen the catalytic activity and stability [22–25]. The stable polyaniline (PANI) not only can serve as a good catalyst support, but also shows promising catalytic activities [26–28]. Therefore, the combination of PANI, CDs and low content of Pt to obtain the composite may be an ideal electrocatalyst with high-efficiency and stability in pH-universal electrolytes for HER.

Here, we demonstrate the carbon dots-Pt modified polyaniline nanosheets grown on carbon cloth (CDs/Pt-PANI) can serve as stable and high-efficient electrocatalyst in pH-universal electrolytes for HER. The CDs/Pt-PANI composite was synthesized by simple electrochemical deposition method. The overpotentials for optimal CDs/Pt-PANI

* Corresponding authors.
E-mail addresses: hhuang0618@suda.edu.cn (H. Huang), mwshao@suda.edu.cn (M. Shao).

https://doi.org/10.1016/j.apcatb.2019.117905
Received 22 March 2019; Received in revised form 24 June 2019; Accepted 25 June 2019
Available online 06 July 2019
0926-3373/

electrocatalyst can be lowered to 30 mV, 56 mV, and 134 mV at 10 mA·cm^{-2} in 0.5 M H_2SO_4, 1 M KOH, 1 M PBS, respectively, when Pt loading is only 8.1 μg·cm^{-2} (the Pt content in commercial 20 wt% Pt/C is 22.4 μg·cm^{-2}), displaying exceptional HER efficiency. Meanwhile, the optimal CDs/Pt-PANI electrocatalyst exhibits well stability with 17 mV potential shift after 20 h, which is 0.06 times than that of commercial 20 wt% Pt/C Pt/C (286 mV) in acidic solution. It should be pointed out that the optimal CDs/Pt-PANI electrocatalyst is superior to 20 wt% Pt/C with HER performance in pH-universal electrolyte (acidic, neutral and basic). Due to the CDs possess abundant surface functional groups, they can connect tightly with PANI and anchor Pt nanocrystal. The activity and stability of electrocatalysts can be improved. Hence, the efficient HER performance should ascribe to the synergy in the CDs, Pt and PANI.

2. Experimental

2.1. Materials

Carbon cloth (CC, 1 × 3 cm^2) was obtained by Aladdin Industrial Co. Aniline (AN) and the commercial 20 wt% Pt/C were obtained from Alfa Aesar Co. Nafion (5 wt%) was obtained from Sigma-Aldrich Co. Other reagents were of analytical reagent grade without further purification. Double-distilled water was used throughout the experiment.

2.2. Materials preparation

2.2.1. Synthesis of CDs-PANI

Sulfonated CDs were synthesized by electrolytic etching method in a reported method [29]. And the content of sulfonic acid groups in CDs was calculated about 4.8%. 2 mg solid CDs was put into 1 mL double-distilled water with continuously ultrasonic treatment to obtain the CDs suspension. The CC was pretreatment by first soaking in the aqua regia for 3 h and then cleaned by distilled water and ethanol, which could enhance its hydrophilia to make it easy for the electrodeposition.

The CDs-PANI composite was synthesized by electrochemical polymerization in 10 mL 0.01 M AN with different contents of CDs at constant current of 0.25 mA·cm^{-2} for 4 min at 30 °C with the CHI 750E electrochemical workstation. A three electrode system was employed in the experiment [30]. The pretreated CC with effective area of 1 × 0.5 cm^2 was used as the working electrode. The reference electrode is saturated Ag/AgCl electrode and the counter electrode is platinum sheet. Through the electrochemical oxidation, AN can convert to PANI with anodic oxidation method. Then the electrode was cleaned by distilled water and ethanol for three times to remove unreacted aniline and CDs on the surface.

2.2.2. Synthesis of CDs/Pt-PANI

The Pt nanocrystals grown on the CDs-PANI composite was electrodeposited with the CHI 750E electrochemical workstation by cathode reduction method. The preparation method was as follows: for CDs/Pt-PANI-4 as example, the electrolyte was composed of 7.7 μmol $H_2PtCl_6{\cdot}6H_2O$, 0.1 mmol $NaH_2PO_4{\cdot}H_2O$ and 10 mL distilled water. The electrodeposition was conducted at the current density of 0.25 mA·cm^{-2} for 20 min. And the as-prepared CDs/Pt-PANI was cleaned by distilled water and ethanol, followed by drying overnight at 60 °C. Other catalysts were prepared in a similar way with different starting materials, which are listed in Table S1 in Supporting Information.

For all pH electrolyte range, the CDs/Pt-PANI-4 tested in 0.5 M H_2SO_4 was named as CDs/Pt-PANI-4 (0), while the CDs/Pt-PANI-4 tested in 1 M PBS solution was named as CDs/Pt-PANI (7), and CDs/Pt-PANI tested in 1 M KOH solution was named as CDs/Pt-PANI (14).

2.2.3. Synthesis of PANI-Na_2SO_4 and PANI-H_2SO_4

For synthesis of PANI-Na_2SO_4, the PANI was grown on the surface of CC by electrochemical polymerization in the 10 mL solution of 0.01 M AN and 1 mmol Na_2SO_4 at constant current of 0.25 mA cm^{-2} for 4 min at 30 °C with the CHI 750E electrochemical workstation.

For synthesis of PANI- H_2SO_4, the Na_2SO_4 was replaced by 400 μL 98% H_2SO_4 as dopant.

2.2.4. Synthesis of Pt-PANI-Na_2SO_4, Pt-PANI-H_2SO_4

For Pt-PANI-Na_2SO_4 and Pt-PANI-H_2SO_4, the preparation methods were similar to that of CDs/Pt-PANI. The Pt was electrodeposited on the PANI-Na_2SO_4 (or PANI-H_2SO_4) with CHI 750E electrochemical workstation by cathode reduction method. Then the Pt-PANI-Na_2SO_4 (or Pt-PANI-H_2SO_4) was cleaned by distilled water and ethanol, followed by drying overnight at 60 °C.

2.3. Characterization

Transmission electron microscope (TEM), high Resolution transmission electron microscope (HRTEM), and energy-dispersive X-ray spectrometry (EDS) of all catalysts were characterized by a FEI Tecnai F20 transmission electron microscope with an accelerating voltage of 200 KV. The SEM of all prepared-materials was characterized by Zeiss G500 scanning electron microscope. Powder X-ray diffraction (XRD) patterns of catalysts were measured by X-ray powder diffraction (XRD, Empyrean), which have Cu Kα radiation source. FTIR spectra were characterized by Microscopic Fourier Transform Infrared Spectrometer with TR procedure. Raman spectra of all catalysts were characterized by Laser confocal microscopic Raman spectrometer (Raman, LabRAMHR800) with laser wavelength of 633 nm. UV–vis spectra were characterized by Ultraviolet visible near infrared spectrophotometer (PE 950). X-ray photoelectron spectroscopy (XPS) information were obtained by Kratos AXIS UltraDLD Ultrahigh vacuum surface analysis system with Al Kα radiation (1486 eV) as a probe and an indium plate as the same holder. The content of catalyst were measured by inductively coupled plasma (ICP-MS).

All electrochemical performance experiments were carried out on the CHI 750E electrochemical workstation with three electrode system. The CC with electrocatalyst was as the working electrode, the saturated calomel electrode (in 1 M PBS and 0.5 M H_2SO_4 solution) or saturated Ag/AgCl electrode (in 1 M KOH solution) were used as the reference electrode and carbon rod as the counter electrode. For 20 wt. % Pt/C, it was loaded on the glassy carbon electrode with diameter of 3 mm (22.4 μg·cm$_{Pt}^{-2}$) and served as the work electrode. In overall water splitting experiment, two-compartment cell with a proton-exchange membrane (Nafion 117, Dupont) was designed. The CDs/Pt-PANI-4 or 20 wt% Pt/C (22.4 μg·cm$_{Pt}^{-2}$) loaded on the CC is served as the cathode and commercial IrO_2 (22.4 μg·cm^{-2}) loaded on the CC is served as the anode. The overall splitting performance was tested in different pH electrolytes with polarization curve at scan rate of 5 mV·s^{-1}. To further measure catalytic performance of as-prepared catalysts, a PEMWE electrolyzer was designed. Graphite bipolar plates are served as current collectors. Two hydrophobic carbon papers (5 × 5 cm^2) were applied as gas diffusion layers (GDLs) in both electrodes. The membrane electrode assembly (MEA) was fabricated by placing a Nafion 117 membrane (5 × 5 cm^2) between CDs/Pt-PANI-4 loaded on CC and IrO_2 (0.1 mg·cm^{-2}) loaded on CC by hot pressing. Double-distilled water was supplied by a peristaltic pump with speed of 14 mL/min. The cell temperature was keep at 60 °C. The PEMWE performance was tested by voltage sweep method at 5 mV·s^{-1}. Subsequently, the measured potentials were calculated against reversible hydrogen electrode (RHE) by the following equation:

$$E\ (\text{vs. RHE}) = E\ (\text{vs. Hg/Hg}_2\text{Cl}_2) + 0.245 + 0.0591\ \text{V} \times \text{pH}$$

$$E\ (\text{vs. RHE}) = E\ (\text{vs. Ag/AgCl}) + 0.197 + 0.0591\ \text{V} \times \text{pH}$$

3. Results and discussion

Scheme 1 illustrates the synthesized process of CDs/Pt-PANI catalysts. The PANI was coated on CC by electrochemical polymerization

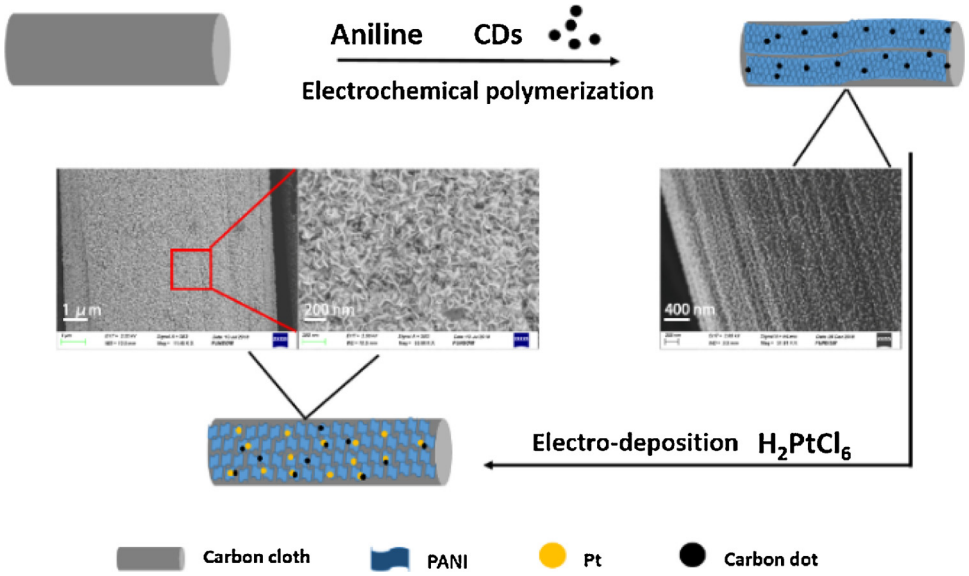

Scheme 1. Schematic diagram for the fabrication of CDs/Pt-PANI.

with sulfonated CDs acting as the dopant. Then Pt nanocrystals were grown on the PANI by electrochemical deposition. Furthermore, CDs provided anchor sites for Pt to improve the connection between active sites and the support. According to a simple two-step method, the CDs/Pt-PANI electrocatalysts were obtained.

3.1. Characterization of electrocatalysts

The SEM images of CC, PANI-H_2SO_4, Pt-PANI-H_2SO_4, Pt-PANI-Na_2SO_4, CDs-PANI and CDs/Pt-PANI-4 are shown in Figure S1. The diameter of the pretreated CC is about 10 μm (Figure S1A). PANI-H_2SO_4 with H_2SO_4 as the dopant exhibits porous structure (Figure S1B). Figures S1C and S1D display the morphologies of Pt-PANI-H_2SO_4 and Pt-PANI-Na_2SO_4 composites. Both of them show the agglomerated Pt with poor dispersity. On the contrary, Figure S1E exhibits the PANI nanoparticles loaded on the CC uniformly, and Figure S1 F shows morphology of the CDs/Pt-PANI-4. As shown, the PANI nanosheets were loaded on the CC uniformly, and no agglomeration of Pt nanocrystals is observed. And Figure S2 is the SEM images of CDs/Pt-PANI with different content of Pt. Their morphologies change with the content of Pt, which should attribute to selective distribution and migration of Pt nanoparticles. For CDs/Pt-PANI-4, PANI nanosheets were supported on the CC become uniformly. When H_2SO_4 and Na_2SO_4 were chosen as dopants, the morphologies of Pt particles also changed with the content of Pt, yet with serious aggregation and uneven distribution (Figures S3 and S4).

To investigate the structure, the TEM and HRTEM images of as-prepared sample were taken. The TEM image of CDs/Pt-PANI-4 (Fig. 1A) reveals that Pt nanocrystals are uniformly grown on the surface of PANI nanosheets with diameter of ~10 nm. Its selected area electron diffraction (SAED) pattern (Fig. 1B) can be indexed as the (111), (200), (220) and (311) diffraction rings of cubic Pt (JCPDS # 04-0802), also confirming the existence of Pt nanocrystals. The diffraction ring of CDs is too weak to be observed. The TEM image of sulfonated CDs is shown in Figure S5, which exhibits fine dispersity with diameter of 3 nm. The HRTEM of CDs/Pt-PANI-4 is shown in Fig. 1C. There is an obvious lattice boundary between the CDs and Pt nanocrystal. The CDs that possess of abundant functional groups help anchor the Pt nanocrystals. The enlarged figure of one area (Fig. 1D) shows the lattice spacing determined to be 0.22 nm, which responses the (111) plane of cubic Pt; and another area (Fig. 1E) exhibits the lattice spacing of 0.21 nm, corresponding to the (100) plane of CDs. Fig. 1F shows the HAADF-STEM image of CDs/Pt-PANI-4. The corresponding EDS mapping (Fig. 1F) reveals the elemental distributions of Pt (green), N (tangerine, coming from PANI), and C (red, coming from PANI and CDs).

Fig. 2A shows the XRD patterns of CC, CDs, CDs-PANI, and CDs/Pt-PANI-4. For curves of CC and CDs, the peaks located at 26°and 44° are assigned to characteristic peaks, which show the (002) and (100) crystal planes of graphite structure [31]. For curves of CDs-PANI and CDs/Pt-PANI-4, The peak of 20° ~ 30° may be assigned to peak of CC, CDs and PANI. And the board peak indicates that PANI film synthesized by electrochemical method is amorphous [32]. Furthermore, in the curve of CDs/Pt-PANI, the diffraction peak of Pt is observed at 39°, corresponding to the (111) crystal plane of cubic Pt (JCPDS # 04-0802). Other diffraction peaks of Pt cannot be observed owing to the low content of Pt. Figure S6A shows the XRD patterns of as-prepared samples with different content of Pt. And Pt-PANI with different dopants display a similar XRD pattern as shown in Figure S6B.

Figure S7 shows the FTIR spectra of sulfonated CDs. The stretching vibration peaks of O—H bond at 3400 cm^{-1}, C═O at 1100 cm^{-1}, and symmetric νs (O═S═O) and asymmetric νas (O═S═O) stretching modes near 1087 cm^{-1} and 1143 cm^{-1} are shown, exhibiting the existence of −COOH and –SO_3H [33,34]. Fig. 2B shows the FTIR spectra of PANI, CDs-PANI, and CDs/Pt-PANI. In the curve of PANI, transmittance peaks at ~1126 cm^{-1} and 1192 cm^{-1} correspond to N═Q═N (Q = quinone) ring vibrations, while the 1487 cm^{-1} and 1568 cm^{-1} are assigned to characteristic peaks of benzene ring, and the one located at ~3487 cm^{-1} is associated with N—H stretching mode of PANI [35]. The broad band between 3400 cm^{-1} may be due to the hydrogen-bond interaction in the composites [36].

Raman spectra of CDs and CC (Fig. 2C, red and black lines) both show two peaks at 1336 cm^{-1} and 1608 cm^{-1}, which belong to the D band because of sp^3 defects, and G band results from in-plane vibration of sp^2 carbon. And for CDs-PANI supported on the CC, the characteristic peaks of PANI are observed (Fig. 2C, blue trace). The peak at around 1328 cm^{-1} belonged to the C-N^+ stretching vibration, and 1442 cm^{-1} attributed to C═N stretching vibration are observed.

UV-Vis absorption spectrum of CDs (Fig. 2D, red line) describes the band around 210 nm is ascribed to π- π* transitions, and the band at 300 nm should result from n-π* transitions, and a broad absorption band around 450 nm can be caused by trapping of excited state energy by the surface states. And in green trace of CDs-PANI (Fig. 2D) shows the characteristic peaks of PANI at 300 nm and 480 nm belong to π-π*

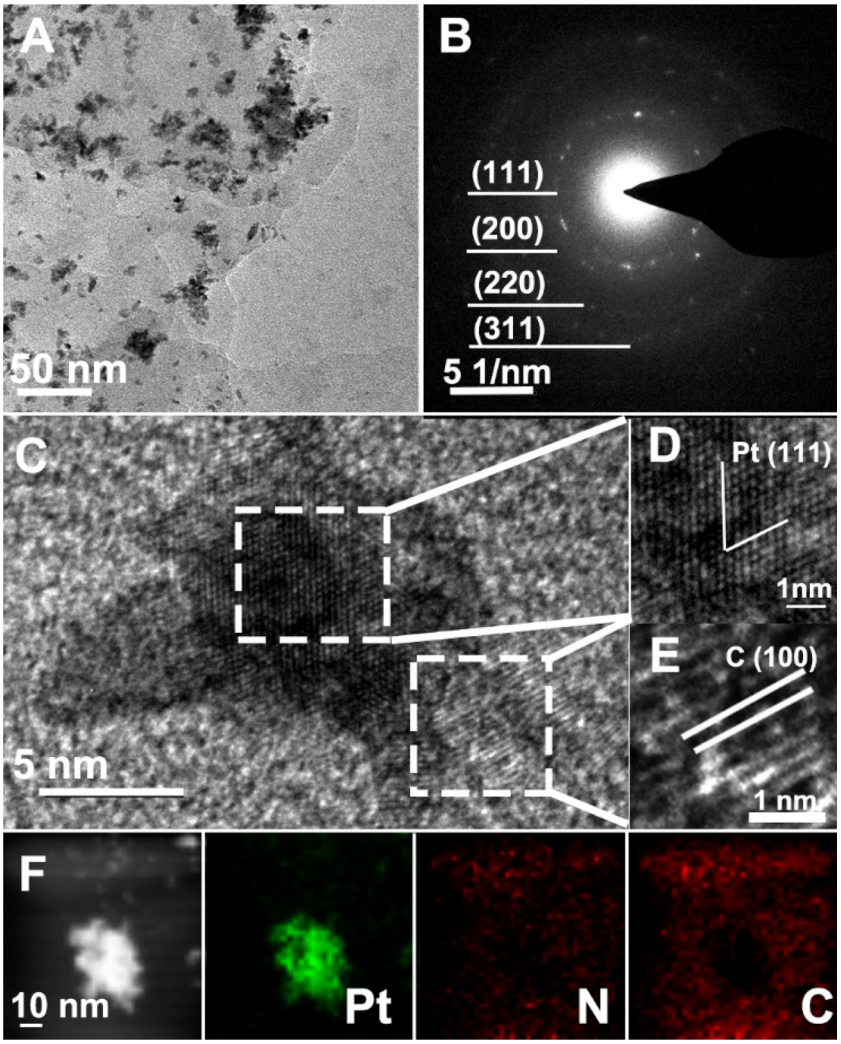

Fig. 1. Characterizations of CDs/Pt-PANI-4: (A) TEM image; (B) SAED pattern; (C) HRTEM image; (D and E) HRTEM images from (C); and (F) HAADF-STEM image and corresponding EDS mapping with Pt (green), N (orange), and C (red) (For interpretation of the references to colour in this figure legend, the reader is referred to the web version of this article).

transition of benzene and quinone. While for the black curve of CDs/Pt-PANI-4 (Fig. 2D), the peak at 230 nm shows the connection of Pt and PANI with the influence of Pt.

To investigate the electron interactions in CDs/Pt-PANI, X-ray photoelectron spectra of CDs-PANI and CDs/Pt-PANI-4 were carried out. Fig. 3A shows the full XPS spectra of CDs-PANI and CDs/Pt-PANI, which indicate the existence of C, N, O, S, Pt elements. Fig. 3B shows the high-resolution C 1s XPS spectra of CDs-PANI and CDs/Pt-PANI-4. As shown, the peaks located at 284.6 eV, 286.0 eV, 287.8 eV corresponding to C—C/C═C, C—N, C—O, respectively for CDs-PANI and CDs/Pt-PANI-4. And Figure S8A shows the high-resolution N 1s spectrum of CDs-PANI. There is three peaks located at ~403.8 eV, ~401.6 eV, ~399.4 eV, corresponding to nitrogen cationic radical, benzenoid amine, and quinoid amine respectively, which could exhibit the existence of PANI [37]. Fig. 3C shows the high-resolution N 1s spectrum of CDs/Pt-PANI-4, where all N peaks of that shifted (~1.36eV, ~1.73 eV, ~1.22eV) to a low binding energy compared with those of CDs-PANI. Fig. 3D shows the XPS spectrum of Pt 4f for CDs/Pt-PANI-4. The peaks at 71.5 and 74.8 eV are assigned to Pt 4f $_{7/2}$ and 4f $_{5/2}$, respectively. The binding energies at 72.9 and 76.2 eV are attributed to Pt-O 4f $_{7/2}$ and Pt-O 4f $_{5/2}$. The Pt 4f $_{7/2}$ peak of CDs/Pt-PANI-4 shows a positive shift (0.7 eV) compared with that of pure Pt/C (70.8 eV) [36]. Figure S8B shows the spectrum of O 1s, and the peak located at 530.4 eV corresponding to Pt-O, which may be originated from the interaction of CDs and Pt. The above results indicate the charge transfer from Pt to CDs and PANI, showing their tight combinations.

The inductively coupled plasma mass spectrometry (ICPMS) measurements reveal a total percentage of Pt in as-prepared catalysts. The loading content of Pt on CC is listed in Table S2 in Supporting Information.

3.2. Electrocatalytic properties

The HER performance of electrocatalysts were conducted by LSV in 0.5 M H_2SO_4 at linear sweep of 5 mV s^{-1}. Figure S9- shows the HER catalytic performance of as-prepared catalysts with different ratio of CDs and AN (volume). When the ratio is 1.5: 1, it exhibits the best activity. Fig. 4A shows the catalysts with different contents of Pt, with the ratio of CDs and AN keeping at 1.5:1. The CDs/Pt-PANI-4 electrocatalyst shows the best HER electrocatalytic performance with the loading of Pt only 8.1 μg·cm^{-2}, which is much less than that of 20 wt% Pt/C (22.4 μg·cm^{-2}_{Pt}). Fig. 4B shows the LSV curves of catalysts using Na_2SO_4, H_2SO_4, and sulfonated CDs as the dopant, respectively. CDs/Pt-PANI-4 shows the best HER performance with lower overpotential (30 mV at 10 m·A cm^{-2}). This illustrates that CDs could promote the dispersion of Pt nanocrystals, increase active sites and accelerate electron transfer. Furthermore, Pt nanoparticles loaded on the substrate uniformly via electrodepositing in suitable concentration of Pt ions.

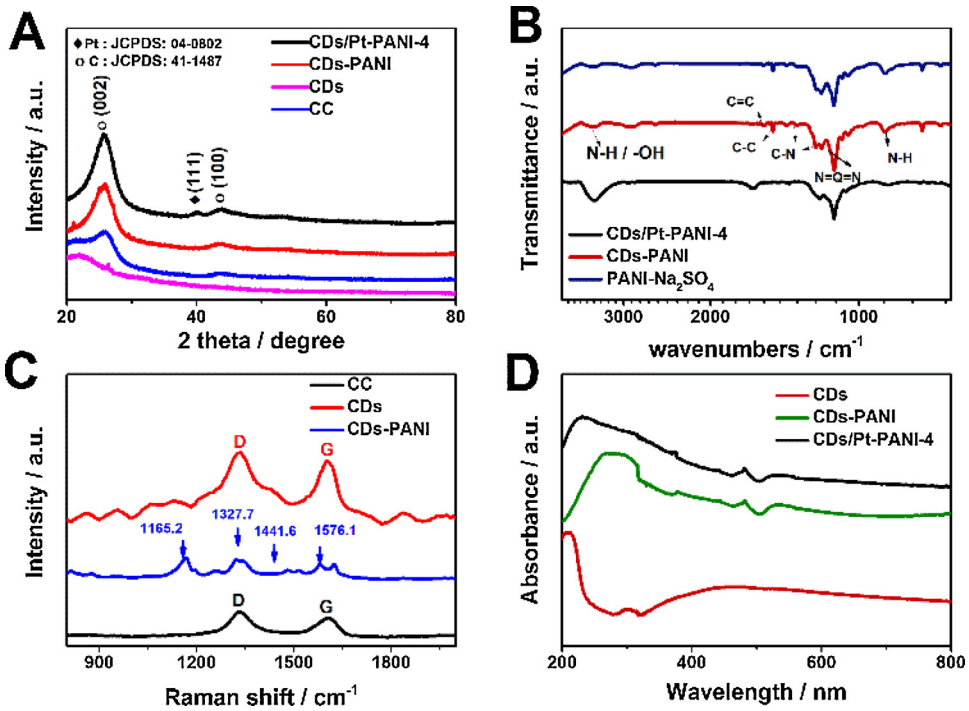

Fig. 2. (A) XRD patterns of CC, CDs, CDs-PANI, and CDs/Pt-PANI-4. (B) FTIR spectra of CDs/Pt-PANI-4, CDs-PANI and PANI-Na_2SO_4. (C) Raman spectra of CC, CDs and CDs-PANI, excited with 633 nm laser beam. (D) UV–vis absorption spectra of CDs, CDs-PANI and CDs/Pt-PANI-4.

Fig. 4C shows the Tafel plots of CDs/Pt-PANI-4, Pt-PANI-Na_2SO_4, Pt-PANI-H_2SO_4, which were derived from the polarization curves from Fig. 4B. The Tafel slope of 41.7 mV dec^{-1} for CDs/Pt-PANI-4 is the smallest one. Fig. 4D shows the mass activity of catalysts, further indicating that CDs/Pt-PANI-4 shows the best activity among all catalysts with different dopants and even surpasses 20 wt% Pt/C. Figure S10 reveals the LSV curves of 20 wt% Pt/C on carbon cloth and GCE. Due to the poor adhesion of Pt/C and carbon cloth, the HER performance of Pt/C on carbon cloth is poor. The comparisons of the HER performance for CDs/Pt-PANI-4 with previous reported Pt-based elecrtocatalysts and non-Pt elecrtocatalysts synthesized by electrodeposited method [38–50] is listed in Table S3, implying the efficient electrocatalytic activity of CDs/Pt-PANI-4.

The electrode kinetics of CDs/Pt-PANI-4 with electrochemical

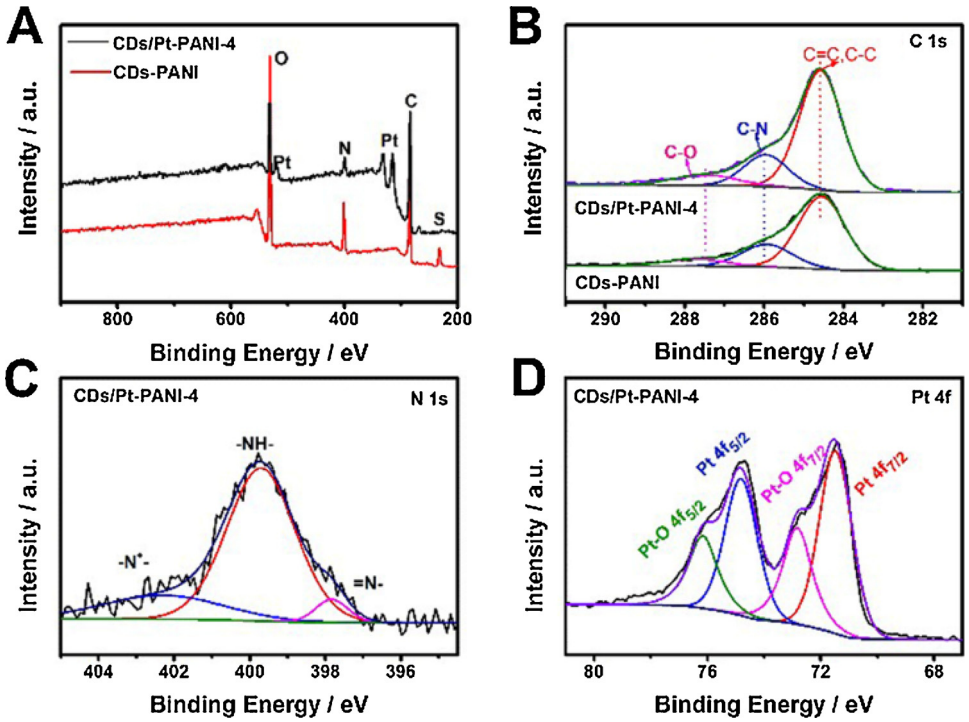

Fig. 3. (A) The full XPS spectra of CDs-PANI and CDs/Pt-PANI-4. (B) High-resolution XPS spectra of C 1s for CDs-PANI and CDs/Pt-PANI-4. (C and D) High-resolution XPS spectra of N 1s and Pt 4f for CDs/Pt-PANI-4.

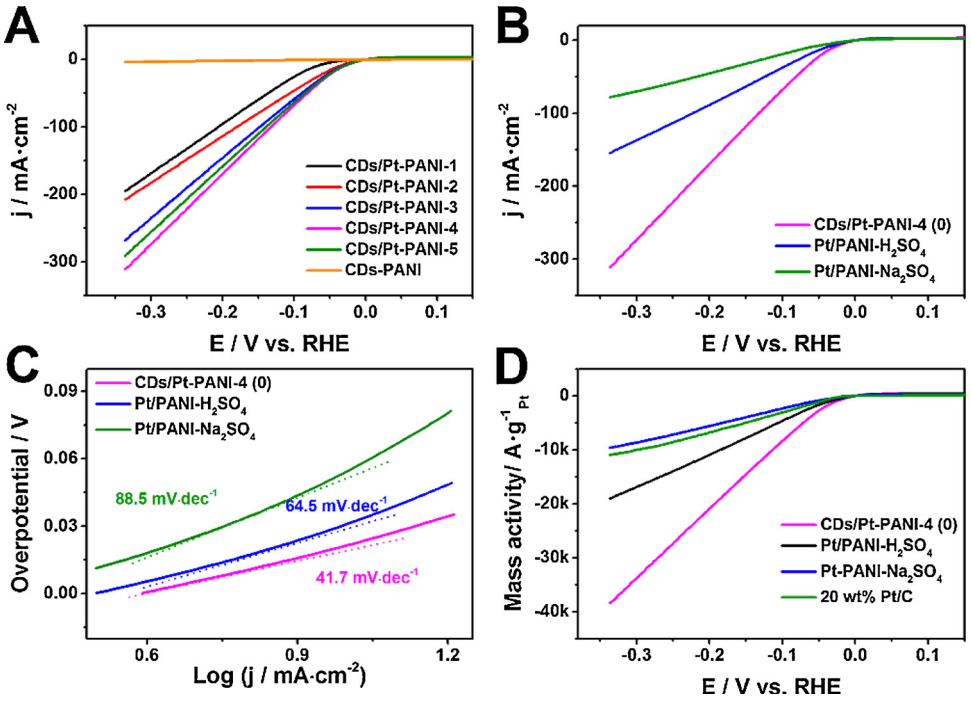

Fig. 4. HER performance of the obtained electrocatalysts: (A) LSV curves of CDs/Pt-PANI with different contents of Pt; (B) LSV curves of Pt-PANI with different dopants (CDs, H_2SO_4 and Na_2SO_4); (C) the corresponding Tafel plots derived from (B); and (D) the mass activity of Pt-PANI with different dopants.

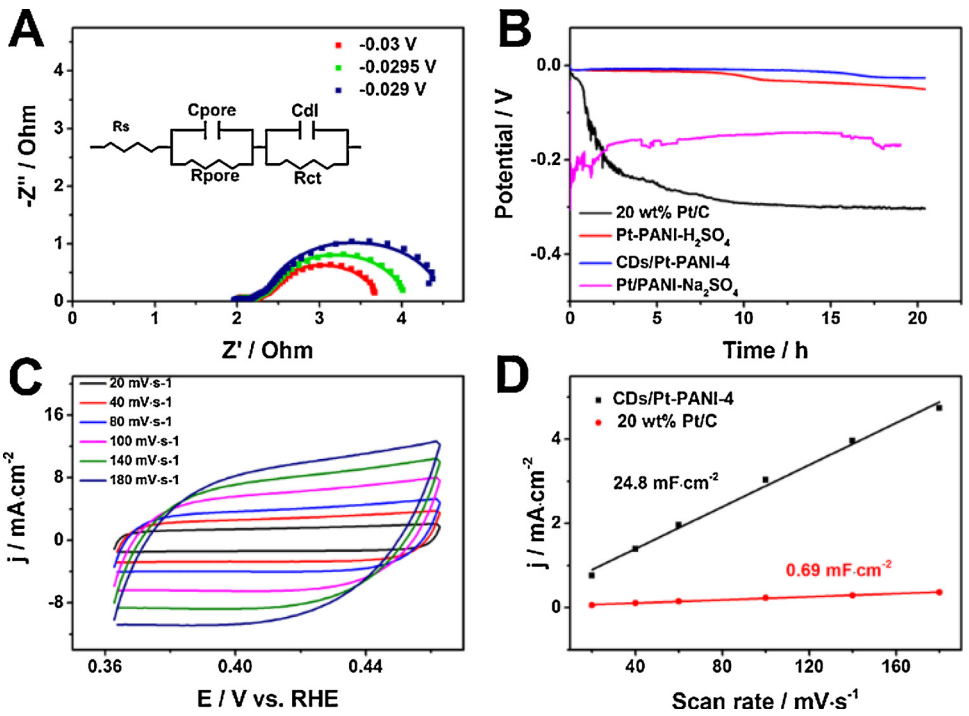

Fig. 5. (A) EIS for CDs/Pt-PANI-4 at different potential. (B) Chronopotential curves of 20 wt % Pt/C and Pt-PANI with different dopants at current density of 10 mA·cm $^{-2}$. (C) CV curves of CDs/Pt-PANI-4 in the region where no faradaic process with the scan rates of 20, 40, 60, 100, 140, 180 mV·s^{-1}. (D) Current density as a function of scan rates for CDs/Pt-PANI-4 and 20 wt% Pt/C.

impedance spectroscopy (EIS) were also employed and shown in Fig. 5A. The Nyquist of catalysts were measured in the frequency ranging from 100 kHz to 0.01 Hz in N_2-saturated 0.5 M H_2SO_4 solution at different potential in the range of -0.029 V to -0.03 V. The equivalent circuit is fitting by the 2TS model (Rs-(Rpore||Cpore)-(Rct||Cdl)): the Cdl-Rct are related to the kinetics of the HER, while Cpore-Rpore mean the porosity of electrode surface. With the increase of overpotentials, the Cdl and Rct decrease. And compared with EIS of 20 wt% commercial Pt/C (Figure S11A), CDs/Pt-PANI-4 exhibits better conductivity. And the EIS spectra of Pt-PANI with different dopants are shown in Figure S11B.

The stability is of crucial importance to excellent electrocatalysts for their practical applications. The chronopotential method was adopted to measure the potential variation with time at a current density of 10 mA cm $^{-2}$. Fig. 5B shows stability of different catalysts measured in 0.5 M H_2SO_4. As shown, the potential shift of 20 wt. % commercial Pt/C is 140 times of that of CDs/Pt-PANI-4 after 10 h; and 20 h later, the potential shift of CDs/Pt-PANI is only 0.017 V, however the 20 wt% Pt/C is 0.286 V. It means that CDs/Pt-PANI-4 shows excellent stability. Figure S12 displays the morphology of CDs/Pt-PANI-4 after 20 h,

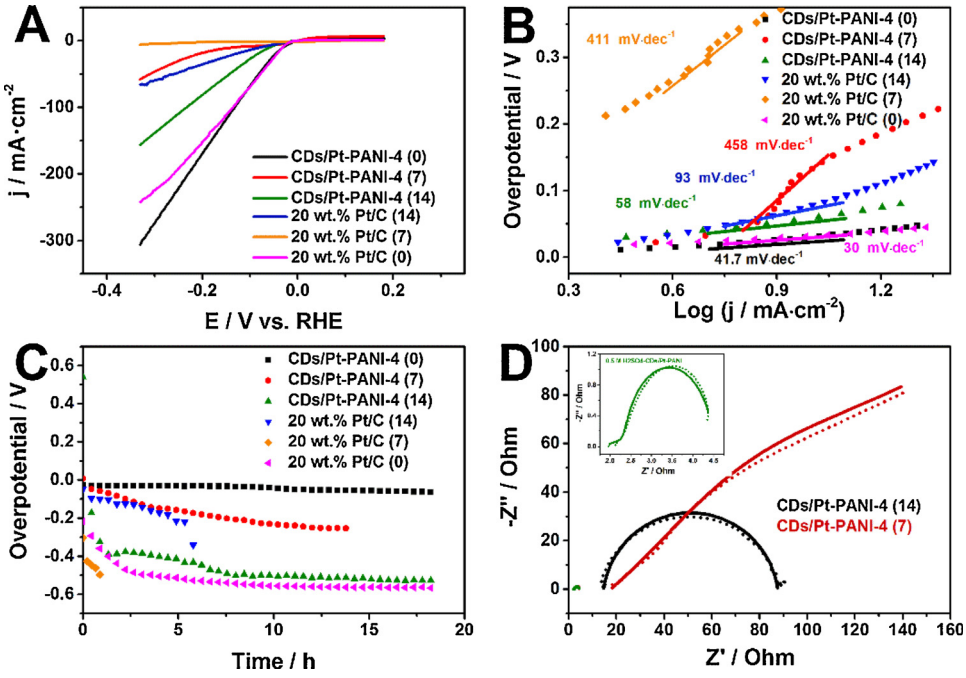

Fig. 6. (A) LSV curves of CDs/Pt-PANI and 20 wt.% Pt/C in 0.5 M H_2SO_4, 1 M KOH, 1 M PBS solution; (B) the corresponding Tafel plots derived from (A); (C) Chronopotential curves of CDs/Pt-PANI and 20 wt.% Pt/C in 0.5 M H_2SO_4, 1 M PBS, 1 MKOH solution; and (D) EIS for CDs/Pt-PANI-4 in 0.5 M H_2SO_4, 1 M PBS, 1 M KOH solution.

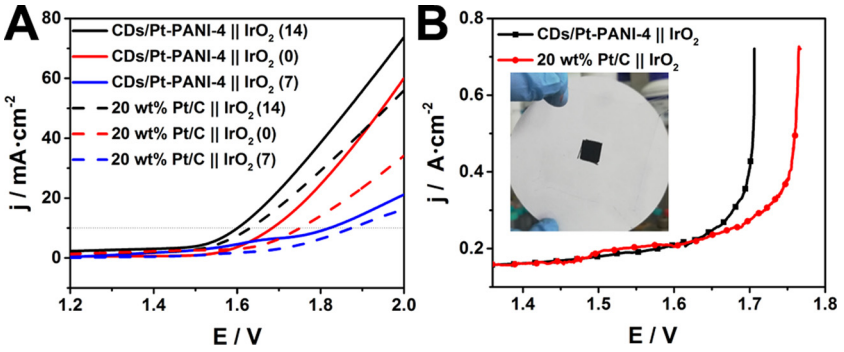

Fig. 7. (A) Overall water splitting performances of CDs/Pt-PANI-4 || IrO_2 and commercial 20 wt% Pt/C || IrO_2 in a 2H-type proton exchange membrane cell with different electrolytes; and (B) polarization curves for the PEMWE electrolyzer with CDs/Pt-PANI-4 || IrO_2 and commercial 20 wt% Pt/C || IrO_2 respectively, at 60 °C. The inset shows the as-prepared membrane electrode assembly (MEA).

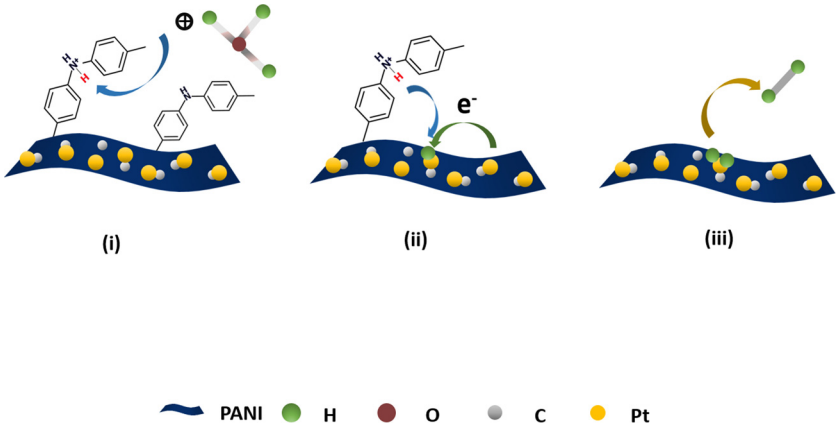

Scheme 2. Schematic diagram for the HER reaction mechanism with CDs/Pt-PANI in acidic solution.

without obvious change, which could illustrate that CDs may increase the stability via playing as a bonding to connect with PANI and Pt.

The C_{dl} was calculated to investigate the effective surface area (ECSA) of samples (Fig. 5C and Figure S13), which is obtained by measuring the capacitance of double layer at solid-liquid interface employing cyclic voltammetry (CV). Fig. 5C shows the CV curves of CDs/Pt-PANI-4. The difference values Δj = (ja-jc)/2 at 0.41 V were used to be plotted against scan rates (Fig. 5D). The C_{dl} of CDs/Pt-PANI-4 (24.8 mF cm $^{-2}$) is much larger than that of 20% commercial Pt/C (1.88 mF cm $^{-2}$). And the larger C_{dl} value of CDs/Pt-PANI indicates the more surface active sites exposed.

The electrocatalysts applied in wide pH electrolyte could broaden their applied range. Therefore, it's worth noting that the HER performance of samples was also characterized in 1 M PBS (7) and 1 M KOH (14) solution. As shown in Fig. 6A, the CDs/Pt-PANI-4 shows higher current density than 20 wt% Pt/C in basic and neutral solution. And

CDs/Pt-PANI-4 (14) requires 56 mV to deliver 10 mA cm $^{-2}$ while 86 mV is required for 20 wt% Pt/C to deliver 10 mA cm $^{-2}$ in 1 M KOH. The Tafel slope of 58 mV dec^{-1} is also smaller than that of 20 wt. % Pt/C (93 mV dec^{-1}) in Fig. 6B. Although the CDs/Pt-PANI-4 (7) shows a lower current density in 1 M PBS solution than those in 0.5 M H_2SO_4 and 1 M KOH electrolyte, CDs/Pt-PANI-4 (7) still presents better HER performance than that of 20 wt% Pt/C in 1 M PBS solution. The results indicate that the CDs/Pt-PANI-4 could keep effectively in basic and neutral electrolyte and shows better HER performance than that of 20 wt % Pt/C in pH-universal solution.

As shown in Fig. 6C, the EIS spectra of CDs/Pt-PANI-4 are characterized in different electrolyte. Meanwhile, the stability of CDs/Pt-PANI-4 was measured in basic and neutral electrolyte. The CDs/Pt-PANI-4 shows better stability than that of 20 wt% Pt/C in the same electrolyte. The potential shift of 20 wt. % Pt/C is 3.5 times of that of CDs/Pt-PANI-4 (14) after 5 h in 1 M KOH. And the potential shift of 20 wt. % Pt/C is 1.4 times of that of CDs/Pt-PANI-4 (7) after 1 h in 1 M PBS solution. The results shows that CDs/Pt-PANI would keep catalytic activity and stability in basic and neutral electrolyte. Furthermore, a two-electrodes system in two-compartment cell with a proton-exchange membrane was made to reveal the overall water splitting performance of CDs/Pt-PANI-4. The CDs/Pt-PANI-4 (or commercial 20 wt% Pt/C) and commercial IrO_2 loaded on the carbon cloth are served as the cathode and anode respectively. Fig. 7A shows overall water splitting performances of CDs/Pt-PANI-4 || IrO_2 and commercial 20 wt% Pt/C || IrO_2 in different electrolytes. As shown, the overall water splitting performance of CDs/Pt-PANI-4 as catalyst in basic electrolyte (black trace) is superior to that of in acidic and neutral electrolytes (red and blue traces), which may due to the poor OER performance of IrO_2 in acidic electrolyte. More importantly, the overall water splitting performance of CDs/Pt-PANI-4 as catalyst is better than that of commercial 20 wt% Pt/C in all electrolytes. To further prominent the performance of CDs/Pt-PANI-4, we compared some reported catalysts with the catalysts we prepared shown in Table S4 [51–54]. To further evaluate the catalytic activity of as-prepared electrocatalyst, cell test was carried out with PEMWE device. The electrolyzer cell design is shown in Figure S14. And Fig. 7B shows the polarization curves of PEMWE electrolyzer with CDs/Pt-PANI-4 || IrO_2 and 20 wt% Pt/C || IrO_2 at 60 °C. When the current density is 720 mA·cm^{-2}, the voltage of CDs/Pt-PANI-4 || IrO_2 electrolyzer and 20 wt% Pt/C || IrO_2 electrolyzer are 1.70 V and 1.76 V respectively.

3.3. Research on electrocatalytic mechanism

Here, high electrocatalytic activity and excellent stability of CDs/Pt-PANI-4 with low Pt content were demonstrated. In order to explain this outstanding HER performance, a possible mechanism in acidic solution is proposed as illustrated in Scheme 2. In HER reaction, the PANI with long electron pairs on N atoms effectively captures H^+ to form protonated amine group, via weakening hydrogen bonding of H^+ ions in the solution. Then the H^+ in the protonated amine groups may easily transfer to the surface of Pt with low transfer barrier, in a similar way as it transfer from PANI to CoP [55–58]. Finally, the H atoms absorbed on Pt react to form hydrogen gas (Scheme 2).

4. Conclusions

We demonstrate the CDs/Pt-PANI electrocatalysts could serve as stable and high-efficient electrocatalyst in pH-universal electrolyte for HER. The optimal CDs/Pt-PANI electrocatalyst (CDs/Pt-PANI-4) shows the excellent catalytic activity with low overpotential of 30 mV at 10 mA·cm^{-2} when Pt loading is only 8.1 μg·cm^{-2}, a small Tafel slope of 41.7 mV·dec^{-1}, and a well stability of 17 mV potential shift after 20 h in acidic solution. Meanwhile, CDs/Pt-PANI shows better HER performance than that of 20 wt% Pt/C in basic and neutral solution. The CDs would connect the PANI and Pt nanocrystal via abundant functional group, which can improved the stability of catalysts. Furthermore, PANI possess abundant electrons on the N atoms derived from amine groups, which can effectively capture H^+ from hydronium ions to form protonated amine groups. Then H^+ transfers from the amine groups to Pt with low transfer barrier. The small and uniformly distributed Pt particles provide numerous active sites and favor the HER catalysis. In addition, CDs were induced for multiple roles: as the dopant to increase the conductivity of catalysts due to sulfate radical on the surface, as the bonder to connect with PANI via forming coordination bonds through functional groups, and as the anchor to fix Pt nanocrystals and keep them from agglomeration during catalysis. Though these advantages, the CDs/Pt-PANI shows excellent HER performance and good stability in pH-universal electrolyte.

Acknowledgements

This work is supported by National Key Research and Development Program of China (2017YFA0204800), National MCF Energy R&D Program (2018YFE0306105), National Natural Science Foundation of China (51725204, 51572179, 21771132, 21471106), the Natural Science Foundation of Jiangsu Province (BK20161216), Collaborative Innovation Center of Suzhou Nano Science & Technology, the Priority Academic Program Development of Jiangsu Higher Education.

Appendix A. Supplementary data

Supplementary material related to this article can be found, in the online version, at doi:https://doi.org/10.1016/j.apcatb.2019.117905.

References

[1] D.B. Pal, R. Chand, S.N. Upadhyay, P.K. Mishra, Renew. Sust. Energy. Rev. 93 (2018) 549–565.
[2] Z.W. Seh, J. Kibsgaard, C.F. Dickens, I.B. Chorkendorff, J.K. Norskov, T.F. Jaramillo, Science 355 (2017) eaad4998.
[3] L.S. Chen, J.L. Shi, J. Mater. Chem. A 6 (2018) 13538–13548.
[4] J. Mahmood, F. Li, S.M. Jung, M.S. Okyay, I. Ahmad, S.J. Kim, N. Park, H.Y. Jeong, J.B. Baek, Nat. Nanotechnol. 12 (2017) 441–446.
[5] Y.X. Chen, K. Yang, B. Jiang, J.X. Li, M.Q. Zeng, L. Fu, J. Mater. Chem. A 5 (2017) 8187–8208.
[6] A.S. Habib, R.M. Babak, A. Elnaz, B. Robabeh, H. Zahra, Chem. Eng. J. 308 (2017) 275–288.
[7] Y.J. Wang, B.Z. Fang, H. Li, X.T. Bi, H.J. Wang, Prog. Mater. Sci. 82 (2016) 445–498.
[8] T. Vu, T.T.T. Tran, H.N.T. Le, L.T. Tran, P.H.T. Nguyen, H.T. Nguyen, N.Q. Bui, Electrochim. Acta 161 (2015) 335–342.
[9] C. Meng, T. Ling, T.Y. Ma, H. Wang, Z.P. Hu, Y. Zhou, J. Mao, X.W. Du, M. Jaroniec, S.Z. Qiao, Adv. Mater. 29 (2017) UNSP 1604607.
[10] R. Kavian, S. Choi, J. Park, T.Y. Liu, H.C. Peng, N. Lu, J.G. Wang, M.J. Kim, Y.N. Xia, S.W. Lee, J. Mater. Chem. A 4 (2016) 12392–12397.
[11] Y.F. Cheng, S.K. Lu, F. Liao, L.B. Liu, Y.Q. Li, M.W. Shao, Adv. Funct. Mater. 27 (2017) 1700359.
[12] P. Jiang, Y. Yang, R.H. Shi, G.L. Xia, J.T. Chen, J.W. Su, Q.W. Chen, J. Mater. Chem. A 5 (2017) 5475–5485.
[13] X.X. Zou, Y. Zhang, Chem. Soc. Rev. 44 (2015) 5148–5180.
[14] J. Li, G.F. Zheng, Adv. Sci. 4 (2017).
[15] J. Wang, F. Xu, H.Y. Jin, Y.Q. Chen, Y. Wang, Adv. Mater. 29 (2017) 1605838.
[16] Y. Zhang, Q. Zhou, J.X. Zhu, Q.Y. Yan, S.X. Dou, W.P. Sun, Adv. Funct. Mater. 27 (2017) UNSP 1702317.
[17] W.C. Xu, S.L. Zhu, Y.Q. Liang, Z.D. Cui, X.J. Yang, A. Inoue, H.X. Wang, J. Mater. Chem. A 5 (2017) 18793–18800.
[18] Y.M. Shi, B. Zhang, Chem. Soc. Rev. 45 (2016) 1529–1541.
[19] Y.H. Lyu, R.L. Wang, L. Tao, Y.Q. Zou, H.J. Zhou, T.T. Liu, Y.Y. Zhou, J. Huo, S.P. Jiang, J.Y. Zheng, S.Y. Wang, Appl. Catal. B-Environ. 248 (2019) 277–285.
[20] Y.Q. Wang, Y.Q. Zou, L. Tao, Y.Y. Wang, G. Huang, S.Q. Du, S.Y. Wang, Nano Res. (2019), https://doi.org/10.1007/s12274-019-2310-2.
[21] D.F. Yan, C.L. Dong, Y.C. Huang, Y.Q. Zou, C. Xie, Y.Y. Wang, Y.Q. Zhang, D.D. Liu, S.H. Shen, S.Y. Wang, J. Mater. Chem. A 6 (2018) 805–810.
[22] T.G. Chatzimitakos, A.I. Kasouni, A.N. Troganis, C.D. Stalikas, ACS Appl. Mater. Interface 10 (2018) 16024–16032.
[23] H.M. Zhang, J.Y. Chen, Y.B. Li, P.R. Liu, Y. Wang, T.C. An, H.J. Zhao, Electrochim. Acta 165 (2015) 7–13.
[24] Z.Y. Shih, A.P. Periasamy, P.C. Hsu, H.T. Chang, Appl. Catal. B-Environ. 132 (2013) 363–369.
[25] Q. Liu, T.X. Chen, Y.R. Guo, Z.G. Zhang, X.M. Fang, Appl. Catal. B-Environ. 193 (2016) 248–258.

[26] W. Wang, Y.M. Kang, J.M. Li, P.D. Wang, X.Y. Liu, Z.Q. Lei, Appl. Surf. Sci. 465 (2019) 979–985.
[27] C.C. Zhao, Y.H. Jin, X. Du, W.B. Du, J. Power Sources 399 (2018) 337–342.
[28] Q. Zhang, Z.H. Yang, Y. Ling, X.X. Yu, Y.F. Zhang, H.S. Cheng, Int. J. Hydrogen Energ. 43 (2018) 12730–12738.
[29] L.P. Wang, X.Q. Wu, S.J. Guo, M.M. Han, Y.J. Zhou, Y. Sun, H. Huang, Y. Liu, Z.H. Kang, J. Mater. Chem. A 5 (2017) 2717–2723.
[30] J.X. Feng, L.X. Ding, S.H. Ye, X.J. He, H. Xu, Y.X. Tong, G.R. Li, Adv. Mater. 27 (2015) 7051.
[31] X.Y. Chen, D.Y. Chen, N.J. Li, Q.F. Xu, H. Li, J.H. He, J.M. Lu, J. Membrane. Sci. 567 (2018) 209–215.
[32] A. Roy, A. Ray, S. Saha, S. Das, Int. J. Hydrogen Energ. 43 (2018) 7128–7139.
[33] U. Baruah, A. Konwar, D. Chowdhury, Nanoscale 8 (2016) 8542–8546.
[34] D. Scholz, O. Krocher, F. Vogel, ChemSusChem 11 (2018) 2189–2201.
[35] K. He, M.T. Li, L.J. Guo, Int. J. Hydrogen Energ. 37 (2012) 755–759.
[36] Y. Sun, Y.J. Zhou, C. Zhu, L.L. Hu, M.M. Han, A.Q. Wang, H. Huang, Y. Liu, Z.H. Kang, Nanoscale 9 (2017) 5467–5474.
[37] D.F. Wu, L.F. Wu, M. Zhang, W.D. Zhou, S. Zhang, J. Polym. Sci. Pol. Phys. 46 (2008) 1265–1279.
[38] Z.L. Wang, K.J. Sun, J. Henzie, X.F. Hao, Y. Ide, T. Takei, Y. Bando, Y. Yamauchi, Mater. Horiz. 5 (2018) 1194–1203.
[39] M. Nadeem, G. Yasin, M.H. Bhatti, M. Mehmood, M. Arif, L.M. Dai, J. Power Sources 402 (2018) 34–42.
[40] A.H. Ghanim, J.G. Koonce, B. Hasa, A.M. Rassoolkhani, W. Cheng, D.W. Peate, J. Lee, S. Mubeen, Front. Chem. 6 (2018) 523.
[41] X.L. Yan, H. Li, J.T. Sun, P.Z. Liu, H.X. Zhang, B.S. Xu, J.J. Guo, Carbon 137 (2018) 405–410.
[42] M.X. Li, Y. Zhu, N. Song, C. Wang, X.F. Lu, J. Colloid Interf. Sci. 514 (2018) 199–207.
[43] R.N. Wasalathanthri, S. Jeffrey, R.A. Awni, K. Sun, D.M. Giolando, ACS Sustain. Chem. Eng. 7 (2019) 3092–3100.
[44] M. Cao, Z. Xue, J.J. Niu, J.Q. Qin, M. Sawangphruk, Y.Y. Zhang, R.P. Liu, ACS Appl. Mater. Interface 10 (2018) 35224–35233.
[45] X.Y. Cao, D.D. Jia, D. Li, L. Cui, J.Q. Liu, Chem. Eng. J. 348 (2018) 310–318.
[46] J. Kim, H. Kim, S.K. Kim, S.H. Ahn, J. Mater. Chem. A 6 (2018) 6282–6288.
[47] S.S. Tao, F. Yang, J. Schuch, W. Jaegermann, B. Kaiser, Chemsuschem 11 (2018) 948–958.
[48] A. Irshad, N. Munichandraiah, ACS Appl. Mater. Interface 9 (2017) 19746–19755.
[49] X. Qian, T. Hang, S. Shanmugam, M. Li, ACS Appl. Mater. Interface 7 (2015) 15716–15725.
[50] J. Zhang, M.D. Baro, E. Pellicer, J. Sort, Nanoscale 6 (2014) 12490–12499.
[51] C. Guan, H.J. Wu, W.N. Ren, C.H. Yang, X.M. Liu, X.F. Ouyang, Z.Y. Song, Y.Z. Zhang, S.J. Pennycook, C.W. Chen, J. Wang, J. Mater. Chem. A 6 (2018) 9009–9018.
[52] Z.L. Chen, H.B. Xu, Y. Ha, X.Y. Li, M. Liu, R.B. Wu, Appl. Catal. B-Environ. 250 (2019) 213–223.
[53] D.T. Tran, H.T. Le, T.L.L. Doan, N.H. Kim, J.H. Lee, Nano Energy 59 (2019) 216–228.
[54] B.B. Cui, B. Hu, J.M. Liu, M.H. Wang, Y.P. Song, K. Tian, Z.H. Zhang, L.H. He, ACS Appl. Mater. Interface 10 (2018) 23858–23873.
[55] H. Xu, A.L. Wang, Y.X. Tong, G.R. Li, ACS Catal. 6 (2016) 5198–5206.
[56] K. He, M.C. Wang, W.B. Wang, R. Miao, W. Zhong, S.Y. Chen, S. Poges, T. Jafari, W.Q. Song, J.C. Liu, ACS Appl. Mater. Interface 9 (2017) 42676–42687.
[57] J.X. Feng, H. Xu, S.H. Ye, G.F. Ouyang, Y.X. Tong, G.R. Li, Angew. Chem. Int. Ed. 56 (2017) 8120–8124.
[58] J.X. Feng, S.Y. Tong, Y.X. Tong, G.R. Li, J. Am. Chem. Soc. 140 (2018) 5118–5126.